applied sciences

MDPI

Article

Application of Improved Process Neural Network Based on the Fireworks Algorithm in the Temperature-Rise Predictions of a Large Generator Rotor

Wu Guo [1,*], Jian Guo [2] and Fengjuan Miao [1]

[1] College of Communication and Electronic Engineering, Qiqihar University, Qiqihar 161000, China
[2] College of Architecture and Civil Engineering, Qiqihar University, Qiqihar 161000, China
* Correspondence: guowu0601@126.com

Abstract: Building an effective algorithm model for large key power equipment has very important research significance and application value. Aiming at the typical operating state characteristics of large generators and taking the temperature changes as the main research indicators, the improved fireworks algorithm was used to optimize the process neural network, and the key data characteristics were studied based on the machine experiment and actual operation data of a 300 MW generator so as to find the variation and development trends of the maximum temperature rise caused by negative-sequence current. Furthermore, the effectiveness of the neural network model suitable for large generators established in this paper was verified by test functions and experiments. On this basis, the calculation method was applied to different working conditions, component materials, and heating positions of the generator. Moreover, the temperature-rise prediction results of the structural components for the generator rotor were obtained, and the optimization scheme of the slot wedge material given, which provide a reference for temperature-rise research and the selection of component materials for large generators.

Keywords: large generator; temperature rise; neural network

check for updates

Citation: Guo, W.; Guo, J.; Miao, F. Application of Improved Process Neural Network Based on the Fireworks Algorithm in the Temperature-Rise Predictions of a Large Generator Rotor. *Appl. Sci.* **2023**, *13*, 2943. https://doi.org/10.3390/app13052943

Academic Editor: Chilukuri K. Mohan

Received: 12 January 2023
Revised: 20 February 2023
Accepted: 22 February 2023
Published: 24 February 2023

Copyright: © 2023 by the authors. Licensee MDPI, Basel, Switzerland. This article is an open access article distributed under the terms and conditions of the Creative Commons Attribution (CC BY) license (https://creativecommons.org/licenses/by/4.0/).

1. Introduction

The temperature rise of large generator rotors in thermal power plants is one of the most important performance indicators when monitoring the status of large power equipment status. Overheating of the rotor will bring great harm to the stable operation of the generator and even the power system [1]. With an increase in generator service time, the increasingly complex power grid structure, overall forging characteristics of the rotor structure, and problems of temperature rise under unbalanced conditions have become increasingly prominent. However, at present, the methods used for the calculation of the negative-sequence temperature rise of large generators have certain drawbacks [2]. In general, the solutions to the negative-sequence problem can be divided into analytical solutions and numerical solutions [3,4]. Analytical solutions are difficult to solve and apply to practical projects and are therefore rarely used in research. The finite-element simulation method has been widely used since the 20th century, but it also has many limitations [5,6]. For example, the finite-element method has the disadvantages of complex calculation, relying on mesh division and material constitutive relations, being a cumbersome and time-consuming process, and the calculation accuracy largely depending on the mesh quality [7]. Although extended finite-element analysis methods have also appeared, these methods are based on the physical level and are limited by the specific structure of the generator; therefore, the calculation result is not ideal [8,9].

The negative-sequence working condition is essentially a dynamic changing process. The whole process changes rapidly and the trend is unpredictable in some cases. In this process, massive system data, equipment data, main parameter change data, and load data

are generated [10–13]. It is obvious that these data are highly time-sensitive and volatile, and require a powerful, high-speed and accurate calculation method for information processing to carry out relevant analysis and calculation of state prediction, equipment evaluation and system optimization operation, and to realize a series of professional operations with strong effectiveness, such as dynamic decision-making and accident handling [14–16]. Therefore, the speed and trend of generator performance change can be obtained to a certain extent, and the approximate trend of negative-sequence temperature rise can be determined through in-depth mining, intelligent calculation of real-time monitoring of characteristic data, and timely prediction of the change trends of rotor temperature rise [17,18]. This is of great significance for monitoring the real-time operation performance and power generation efficiency of large generators, saving maintenance costs and reducing the failure rate of generators.

Nowadays, the increasing unit capacity of generators, as well as the corresponding increased electromagnetic load and thermal load, can easily cause local heating inside turbo-generators [19–21]. With the continuous increase in generator capacity, their volume also becomes larger and larger, and most rotors use an integral forged structure, as shown in Figure 1, which makes the harm caused by asymmetric operation more serious. At present, research on the experimental and numerical calculations of the rotor is still expanding. The dynamic balance of a rigid variable speed rotor has been tested and analyzed [22]. For an in-line arrangement of two drag-type hydrokinetic rotors, flow patterns between the two rotors and the rotor performance were investigated [23]. In [24], a novel rotor design provided better efficiency with less rotor loss but showed the disadvantage of a decreased power factor. The use of space vectors and symmetrical components of instantaneous values of currents and voltages was studied in [25]. However, classical methods still have shortcomings in computing speed, fast real-time fault processing, and online prediction evaluation for large dynamic systems under asymmetric conditions.



Figure 1. Example of a rotor of a synchronous generator of hundreds of MVA.

The development and evolution of intelligent computing methods have led to great progress in the application of many industrial technology fields and provides the possibility to solve complex engineering problems [26–28]. A synchronous generator connected to a smart grid was improved by the novel recurrent Chebyshev neural network and amended particle swarm optimization to avoid the generation of negative-sequence currents in [29]. A new control strategy was proposed to minimize the significantly unbalanced effect caused by the negative-sequence component on the voltage and current of the power winding during the unbalanced operation of a generator in [30]. To overcome the shortage of cooling technology to manage the overheating of large generator rotors, the impacts of cooling modes, operating parameters, and ambient conditions were investigated in [31].

In order to further improve the calculation accuracy and prediction accuracy of the process neural network, this paper improves the fireworks algorithm (FWA) at the same

time and applies the improved algorithm to the process neural network to optimize the network parameters and realize the effective monitoring and analysis of the different working conditions of the generator. Inspired by the physical phenomenon of fireworks generating sparks around the explosion center in the night sky, Tan et al. proposed the FWA [32]. Compared with the genetic algorithm and particle swarm optimization algorithm, the FWA shows a different search mechanism by adopting an explosion search mechanism, calculating the explosion radius and the number of sparks of each firework through the interaction mechanism, so that fireworks with good fitness value obtain more resources; on the contrary, fireworks with poor fitness value obtain fewer resources [33,34]. The FWA has the ability to balance the global search and local search, but the traditional FWA also has defects, such as high time complexity, mainly because the firework explosions produce a large number of explosion sparks; with the increase in the number of iterations, the calculation cost becomes higher, and the Euclidean distance is used in the selection strategy to calculate the distance between any two individuals, which consumes a lot of time [35]. There is a lack of information on the interaction mechanisms between fireworks and explosion sparks. Due to the lack of utilization of optimal firework information, the population diversity decreases with the increase in iteration times, so it is easy to fall into local optimality and other shortcomings.

The Loser-Out Tournament-Based Fireworks Algorithm (LoTFWA) is a multimodal fireworks algorithm based on the elimination of losers as proposed by J. Li and Y. Tan in 2018 [36], which introduces a loser elimination mechanism. First, it predicts the fitness value of the ith fireworks in the final generation and, then, compares it with the fireworks with the best fitness of the current generation. If the value is inferior to the best fitness value of the current generation, it is considered that the fireworks have failed and are thus reinitialized; that is, a new position is randomly generated in the search space, and its explosion amplitude is set to the initial value. This makes the algorithm search more promising areas so as to enhance the local search ability of the algorithm. This algorithm not only avoids searching the same region many times but also avoids searching regions with poor prospects. The LoTFWA improves the generation equation and selection strategy of explosive sparks. The experimental results show that its search effect is far better than other typical improved FWAs, especially in multimodal functions, where its advantages are more prominent, and good optimization results are obtained. However, the LoTFWA adopts random mapping rules, which makes it easy to lose the original characteristics of sparks in the mapping process. In order to overcome this shortcoming, this paper proposes an improved FWA to more effectively balance the global and local search capabilities of the algorithm.

On this basis, this paper proposes a process neural network prediction model based on the improved FWA. The algorithm is compared by using the actual operation data of the generator and the experimental results, combined with the standard test function, showing the effectiveness of the proposed algorithm. At the same time, aiming at the typical problems of large generators under different working conditions, the data analysis and calculation under the premise of steady-state asymmetric operation are carried out to explore the change law of different slot wedge materials for the maximum temperature rise caused by electromagnetism of the generator rotor, predict the key parts of the rotor heating, and obtain the characteristics of the influencing factors of the maximum temperature rise of the generator.

2. Requirements on Computing and Data Resources of Large Generator Operation States

The running states of steam turbines, generators, transformers, instrument current transformers, instrument voltage transformers, circuit breakers, and other different power generation equipment and power supply equipment directly determines the vital interests of users. Therefore, how to measure the operation states of large power equipment has become an urgent technical problem to be solved.

2.1. Composition of Data Processing System

From the actual situation, the power plant online data processing system is composed of four parts, namely, the data sensing layer, data transfer layer, data computing layer, and data application layer; the details and main construction are given in Figure 2.

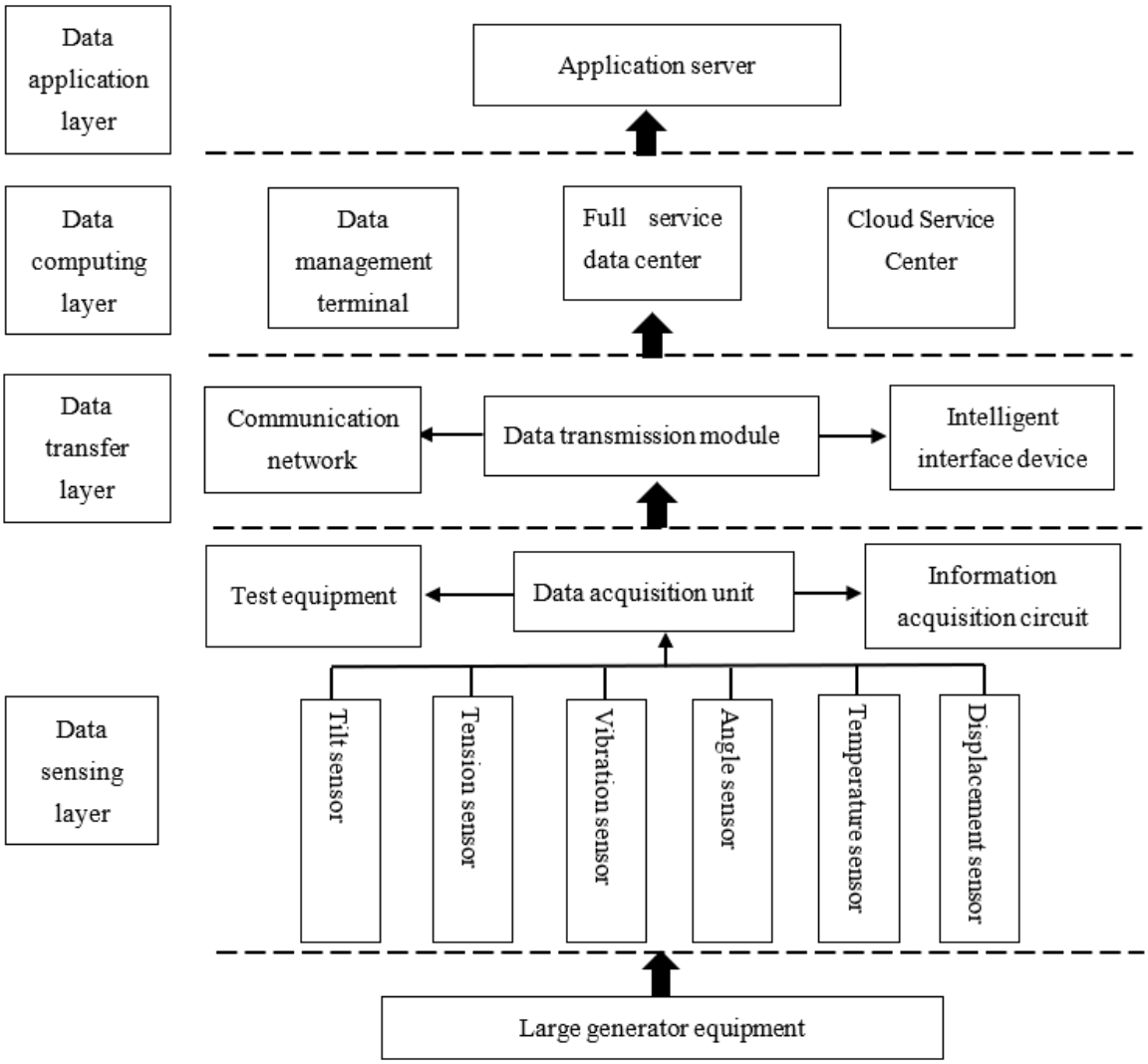


Figure 2. Online data processing system of generator.

It can be seen from Figure 2 that an intelligent algorithm plays an irreplaceable role in the data processing power and provides a favorable technical guarantee for the development of computing technology for large equipment in the future. First of all, as the bottom layer, the data sensing layer undertakes the important task of data information collection and processing, mainly using vibration and temperature and humidity sensors to check power equipment and realize data information sharing and data fusion. Secondly, the data transfer layer mainly uses the wide area network, sensor network, and communication network to receive the information transmitted by the sensing layer and transmit the information to the data computing layer, connecting the data sensing and data computing layers. Thirdly, the data computing layer is the key of the power plant data processing system. It can effectively and accurately calculate a large amount of data information and conduct unified management to strengthen the efficiency of online data analysis and processing. Finally, the data application layer is the interface between the system and users, which can receive system information, comprehensively process information, strengthen the online monitoring of power equipment, and provide management services.

2.2. Difficulties in Intelligent Computing of Operation Data

The state prediction of a large generator mainly uses detection means and analysis and diagnosis technology to master the operation state and enhance the safety and reliability of operation. The main purpose of generator condition estimation is to find hidden dangers and faults in the operation process in time and reduce the probability of major problems. In the process of operation, the power generation quality is affected by the load of aspects such as electricity, heat, and machinery, in addition to the environment, which may lead to aging, wear, performance degradation, and other problems. At the same time, the performance of the main component materials will also decline due to the influence of high temperature, high pressure, and other factors. The occurrence of these conditions may lead to generator failure and potential safety hazards, so it is necessary to strengthen state calculation in a timely manner when an alternating magnetic field causes an eddy current loss in the solid parts that can produce or cause overheating. The operating parameters of the equipment can be obtained through sensors to reflect the running state of the equipment. However, in recent years, the running conditions of generators have become more and more complex, and the data types have become more diverse. Traditional mathematical algorithms cannot guarantee the efficiency and quality of data processing.

In addition, the generator needs to monitor the surface temperature of its stator and rotor, especially the surface temperature at the position where the electromagnetic eddy current loss can easily occur at the connection of various structural parts [37,38]. During operation, the generator carries a high line load, so even with a good ventilation system, more additional losses will be generated inside the generator under asymmetric operation, resulting in temperature rising more seriously in the main structural parts of the rotor [39]. Therefore, the surface area of the rotor is the top priority in research on temperature rise, which requires that the generator be able to bear a certain amount of unbalanced energy. The eddy current density forms on the rotor surface and the heat generated depends largely on the specific structure of the rotor itself. If the rotor body produces a large temperature-rise gradient, then any uneven expansion, elongation, or deformation will inevitably cause damage to the generator rotor, and in serious cases, cracks may appear, greatly reducing its fatigue life [40,41]. The state data of the generator include the current and voltage recording data of three-phase lines and neutral lines, infrared data, ultraviolet data, and visible light tilt photography data (which provide a reference for infrared and ultraviolet data) as shown in Figure 3.

At least three voltage acquisition systems, four current acquisition systems, n visible light cameras, n infrared cameras, and n ultraviolet cameras need to be deployed. In this way, the voltage and current oscillogram information of the generator, the rotor temperature information, the creep state positioning information based on the three-dimensional real-time model, the arc and micro-arc positioning information, and the integration information of the load state are obtained.

In the smart grid, circuit breaker devices are configured at the generator outlet to ensure the disconnection operation in case of system failure. Therefore, circuit breaker-related data are an essential part in the process of information collection, as shown in Figure 4.

The redundant data extracted from the three sets can carry out 3D tilt photography and imaging of the switch, determine the positioning of the corresponding mechanism and arc positioning, and capture the temperature information of the contact and non-line parts at the same time. The levels of detail (LOD) of the switch state are transferred to the real-time 3D model. At the same time, the switch action information, switch value information, and positioning information are obtained.

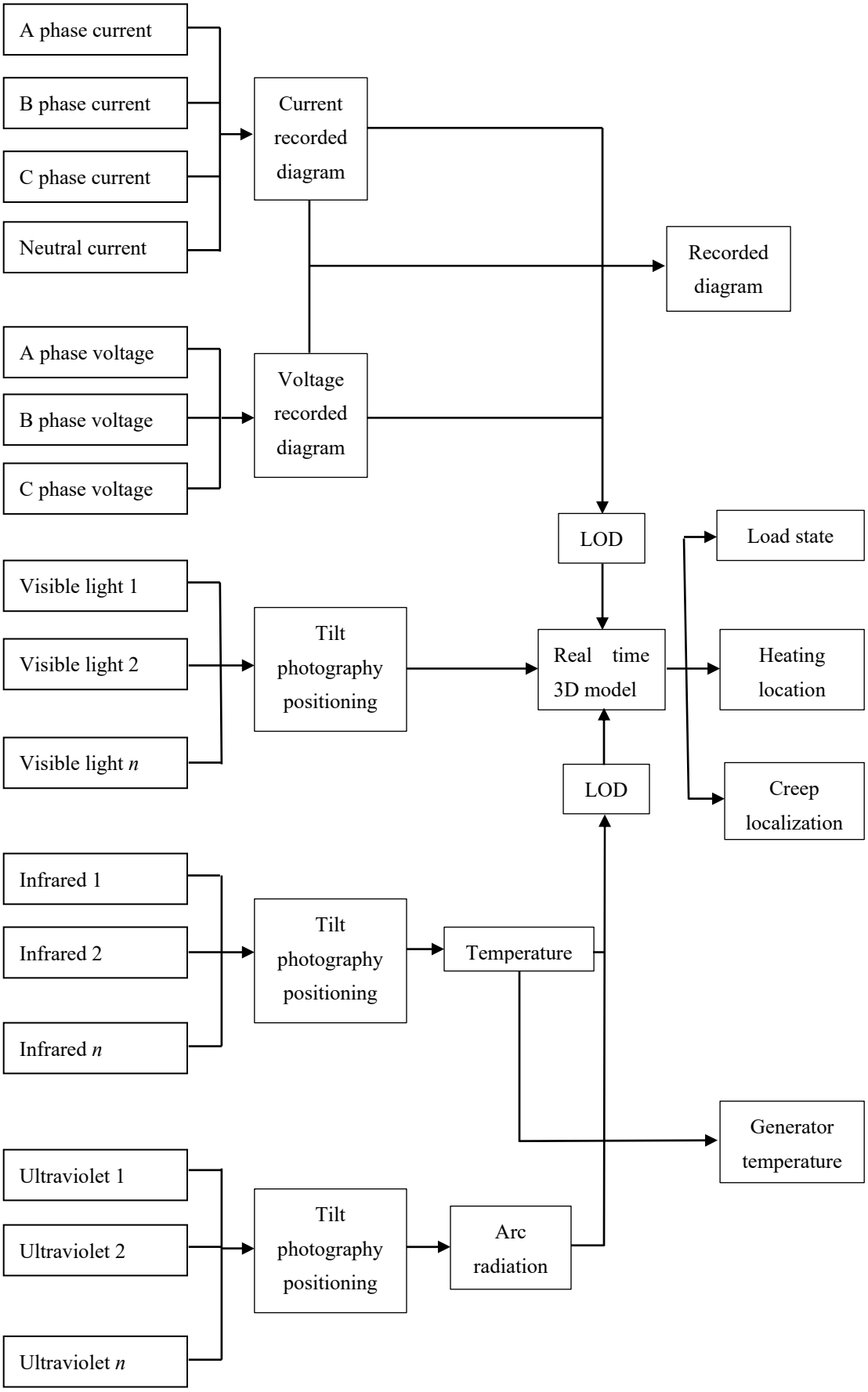


Figure 3. Data collection for large generator.

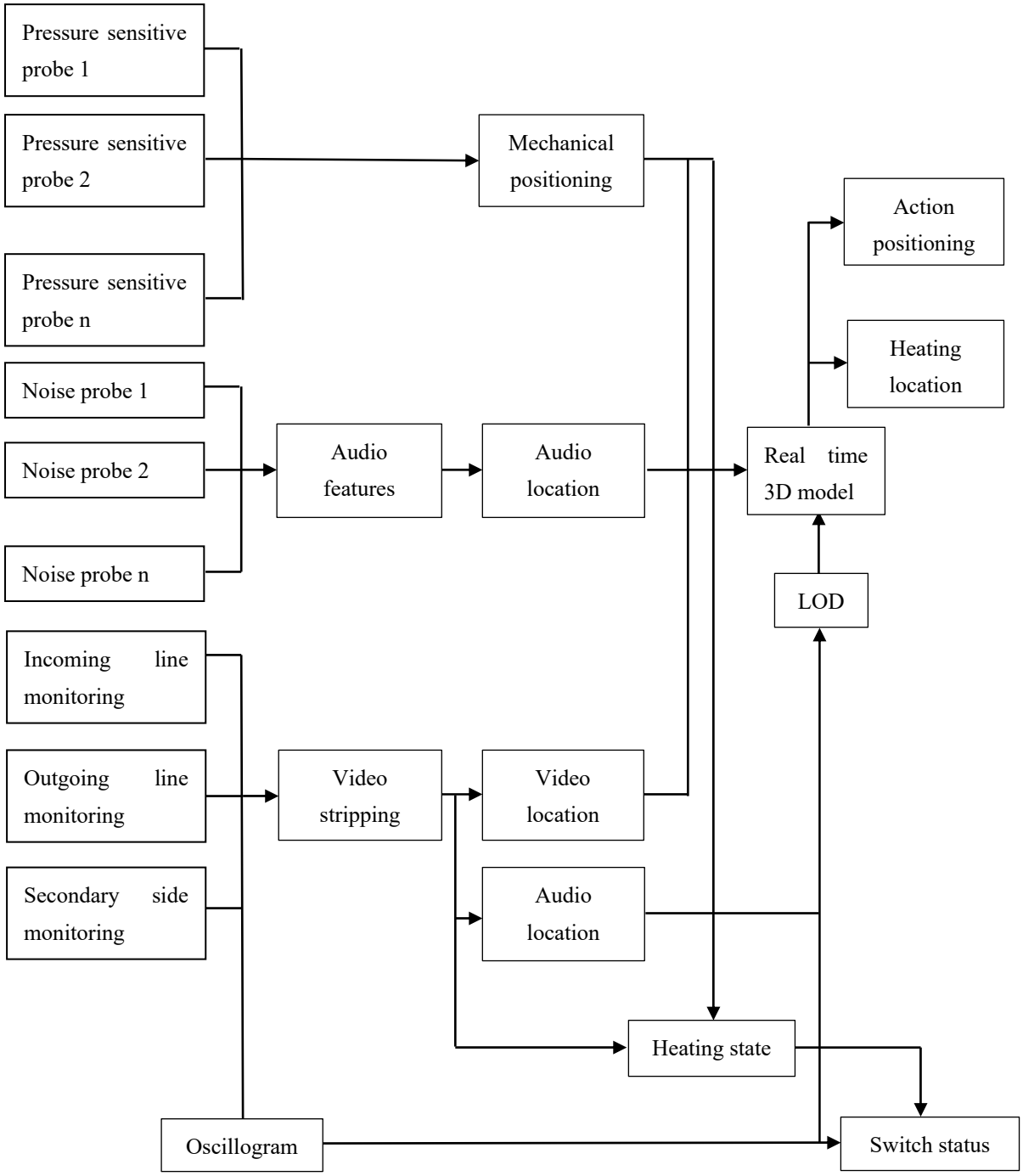


Figure 4. Data collection for generator outlet circuit breaker.

Through the above analysis of the generator data acquisition process, it can be seen that the amount of data collected during operation is very large, and there is a large amount of redundant information, while the monitoring and prediction evaluation research needs to quickly capture and calculate the characteristic data. In addition, the generator is a large piece of power equipment requiring long-term stable operation, and the time cumulative effect should be considered in the change law of main parameters. Hence, it is necessary to study how to explore the time-domain characteristics of the data from the current time node and historical time node combined with multi-source data, so as to realize the prediction of the future state of the equipment in advance.

3. Proposal and Verification of Improved LoTFWA

The LoTFWA, based on the elimination of losers, is one of the best improved FWAs proposed at present. This paper mainly improves the explosion operator, and its experimental results on 24 standard test functions are shown to be better than other improved FWAs.

3.1. Classic Algorithm of LoTFWA

The LoTFWA has improved the equation for generating the number of explosive sparks in the FWA. The power distribution equation is used to generate the number of explosive sparks, and its generation equation is shown in Equation (1).

$$\lambda_i = \hat{\lambda} \cdot \frac{r_i^{-\alpha}}{\sum_{i=1}^{m} r_i^{-\alpha}}, \tag{1}$$

where r_i is the fitness value ranking of the ith fireworks; m is the total number of fireworks; α is the parameters of explosive spark distribution shape, and a better explosion effect is obtained when α is larger; and $\hat{\lambda}$ is a parameter that controls the number of sparks. In previous improved FWAs, only the best explosion amplitude of fireworks was dynamically controlled. However, the dynamic control is added to the explosion amplitude of each firework in the LoTFWA, and its explosion amplitude improvement publicity is shown in Equation (2).

$$A_i^g = \begin{cases} A_i^1 & g = 1 \\ C_r A_i^{g-1} & f\left(x_i^g\right) \geq f\left(x_i^{g-1}\right) \\ C_\alpha A_i^{g-1} & f\left(x_i^g\right) < f\left(x_i^{g-1}\right) \end{cases} \tag{2}$$

where A_i^g is the explosion amplitude of the ith fireworks in the g generation and x_i^g is the position of generation g of the ith fireworks. When g generation fireworks are better than generation $g-1$ fireworks, multiply by the amplification factor $C_\alpha > 1$ ($C_\alpha = 1.2$); otherwise, multiply by the reduction factor C_r ($C_r = 0.9$) so that the best fireworks enter the next generation.

The explosion spark generation equation of the LoTFWA is shown in Equation (3).

$$S_{ij}^{(k)} \leftarrow X_i^k + \eta \cdot A_i, \tag{3}$$

where X_i^k is the position of the ith fireworks X_i in the kth dimension of the explosion space; $S_{ij}^{(k)}$ is the position of the jth explosion spark generated by fireworks X_i in the kth dimension; Ai is the explosion amplitude of the ith fireworks; and η is a uniformly distributed random number in $(-1, 1)$.

When the explosion sparks and Gaussian variation sparks generated in the explosion operation exceed the boundary of the feasible region, the explosion sparks and Gaussian sparks are mapped into the feasible region by mapping rules. The equation is shown in Equation (4).

$$\overline{X}_i^k = LB + rand * (UB - LB), \tag{4}$$

where $\overline{X}_i^k$ is the new location of the explosion space; UB and LB are the upper and lower boundaries of the explosion space; and rand means to generate a random number from 0 to 1.

The traditional firework selection framework is to add the current fireworks, the generated explosion sparks and the Gaussian variation sparks into a candidate pool from which n solutions are selected as the next generation of fireworks. The LoTFWA uses the independent selection fireworks framework; that is, each firework has an independent candidate pool, and the next-generation fireworks are also selected from their respective candidate pools. The LoTFWA adopts a combination of greedy selection and elite selection

mechanisms, and selects m fireworks from the current generation of fireworks, explosive sparks, and Gaussian variation sparks as the next generation of fireworks.

3.2. Improved LoTFWA Based on Location Feature Mapping Rules

The mapping rule in the traditional FWA adopts the remainder operation, which can easily map the explosive sparks, and Gaussian sparks near the origin. For a function whose optimal value is at or near the origin, this method can help the FWA quickly converge to the optimal value. However, for a function whose optimal value is far away from the origin, this method maps most sparks beyond the boundary to the position around the origin far away from the optimal solution. Instead, this increases the difficulty of optimization. In order to overcome this defect and prevent the sparks after mapping from gathering near the origin, the LoTFWA algorithm maps the sparks beyond the boundary to any point in the feasible region through the uniform random mapping rule of Equation (4). However, this method does not consider the relative position relationship between the generated spark and the upper and lower bounds of the feasible region, and does not retain the position characteristics of the generated spark. Moreover, it completely discards the information generated by the spark explosion process and randomly generates a new spark in the feasible region, which has great blindness. In order to solve this problem, this paper proposes a new mapping rule considering the position characteristics: when the spark exceeds the upper boundary of the explosion space, use Equation (5) to map the spark evenly and randomly to the region from two-thirds of the feasible region to the upper boundary; when the spark is lower than the lower boundary of the explosion space, use Equation (6) to map the spark evenly and randomly to the area from the lower boundary to two-thirds of the feasible region.

$$\overline{X}_i^k = UB - rand * (UB - (UB + LB)2/3), \tag{5}$$

$$\overline{X}_i^k = LB + rand * ((UB + LB)2/3 - LB), \tag{6}$$

where UB and LB are the upper and lower boundaries of the explosion space, respectively. The mapping rules of the Improved LoTFWA (ILoTFWA) proposed in this paper effectively extract the position information generated after spark explosion and map the sparks beyond the boundary more pertinently. This not only increases the diversity of the population compared with the traditional residual mapping rule but also enhances the pertinence of the mapping position compared with the random mapping rule of the LoTFWA and retains the relative position between the generated spark and the boundary to a certain extent, which improves the search efficiency of the FWA and helps to speed up the convergence speed of the algorithm.

3.3. Validation and Analysis of ILoTFWA

In order to verify the effectiveness of the ILoTFWA proposed in this paper, 24 functions in the CEC2013 test function set were used for simulation experiment analysis, of which 2 were unimodal functions (f_1~f_2), 14 were multimodal functions (f_3~f_{16}), and 8 were composite functions (f_{17}~f_{24}). The specific names of functions are shown in Table 1. The overall improvement effect and superiority were tested among the ILoTFWA, LoTFWA, and several other improved FWAs.

The parameter setting of the ILoTFWA proposed in this paper is the same as that of the LoTFWA: the number of fireworks m = 5, the initial value of the parameter of the number of explosive sparks generated $\hat{\lambda}_i^0$ = 300, dynamic amplitude scaling factor C_α = 1.2, C_r = 0.9, scaling factor S_α = 1.2, S_c = 0.8 for adaptive adjustment of explosion spark quantity parameters, Gaussian variation adaptive control parameters σ = 0.2, and the dimension of search space of all test functions d = 30. The maximum evaluation time is 300,000, and it runs 51 times independently on each function.

Table 1. The 24 test functions.

Function Type	No.	Function Name
Unimodal function	1	Rotated Discus Function
	2	Different Powers Function
Multimodal function	3	Rotated Rosenbrocks Function
	4	Rotated Schaffers F7 Function
	5	Rotated Ackleys Function
	6	Rotated Weierstrass Function
	7	Rotated Griewanks Function
	8	Rastrigins Function
	9	Rotated Rastrigins Function
	10	Non-Continuous Rotated Rastrigins Function
	11	Schwefel's Function
	12	Rotated Schwefel's Function
	13	Rotated Katsuura Function
	14	Lunacek Bi Rastrigin Function
	15	Rotated Lunacek Bi Rastrigin Function
	16	Expanded Griewanks plus Rosenbrocks Function
Composite function	17	Composition Function 1 (Rotated)
	18	Composition Function 2 (Unrotated)
	19	Composition Function 3 (Rotated)
	20	Composition Function 4 (Rotated)
	21	Composition Function 5 (Rotated)
	22	Composition Function 6 (Rotated)
	23	Composition Function 7 (Rotated)
	24	Composition Function 8 (Rotated)

The ILoTFWA was also compared with the classical FWA and other improved FWAs that have performed well in recent years. The three comparison algorithms include: the adaptive fireworks algorithm (AFWA) [42], cooperative fireworks algorithm (CoFWA) [43], and guiding fireworks algorithm (GFWA) [44]. The parameters of these algorithms were set to the values recommended in the original paper and were consistent with the corresponding parameters of the algorithm proposed in this paper. Their means and standard deviations are shown in Table 2, and the bold part indicates that the mean was the best among all comparison algorithms.

It can be seen from Table 2 that the existing algorithms, the AFWA and GFWA, performed best in the optimization of unimodal functions. Among the multimodal functions (f_3~f_{16}) and composite functions (f_{17}~f_{24}), the error of the ILoTFWA was the smallest; that is, its overall search performance was the best among all the fireworks algorithms compared, and the LoTFWA algorithm was the second. It can also be seen that the ILoTFWA was significantly better than the existing improved FWAs in most multimodal functions. The above experimental results show that the improved mapping rules designed by the ILoTFWA based on the LoTFWA algorithm are feasible and effective. They can further improve the search efficiency of the algorithm in complex optimization problems such as multimodal functions and composite functions, so as to effectively promote the accuracy of solving problems such as multivariable feature extraction in complex physical processes.

Table 2. Mean and standard deviation comparison results of ILoTFWA and other FWA algorithms.

Function No.	FWA		AFWA		CoFWA		GFWA		LoTFWA		ILoTFWA	
	Mean	Std	Mean	Std	Mean	Std	Mean	Std	Mean	Std	Mean	Std
1	1.21×10^{0}	3.64×10^{-1}	1.17×10^{1}	6.92×10^{0}	2.43×10^{3}	1.56×10^{3}	$\mathbf{5.07 \times 10^{-5}}$	6.24×10^{-5}	2.61×10^{3}	8.35×10^{2}	1.23×10^{3}	6.69×10^{2}
2	8.59×10^{-2}	1.68×10^{-2}	$\mathbf{6.11 \times 10^{-4}}$	9.37×10^{-5}	7.37×10^{-4}	9.68×10^{-5}	1.61×10^{-3}	1.94×10^{-4}	3.69×10^{-5}	5.25×10^{-4}	5.12×10^{-3}	1.41×10^{-3}
3	5.69×10^{1}	3.74×10^{1}	2.86×10^{1}	2.54×10^{1}	2.52×10^{1}	2.13×10^{1}	3.58×10^{1}	2.82×10^{1}	$\mathbf{1.48 \times 10^{1}}$	6.91×10^{0}	1.62×10^{1}	4.21×10^{0}
4	1.45×10^{2}	4.68×10^{1}	9.27×10^{1}	2.71×10^{1}	9.13×10^{1}	1.95×10^{1}	7.67×10^{1}	3.06×10^{1}	5.14×10^{1}	9.73×10^{0}	$\mathbf{3.18 \times 10^{1}}$	1.01×10^{1}
5	2.36×10^{1}	4.98×10^{-2}	$\mathbf{2.08 \times 10^{1}}$	7.83×10^{-2}	$\mathbf{2.08 \times 10^{1}}$	9.75×10^{-2}	$\mathbf{2.08 \times 10^{1}}$	9.10×10^{-2}	$\mathbf{2.08 \times 10^{1}}$	6.12×10^{-2}	$\mathbf{2.08 \times 10^{1}}$	6.71×10^{-2}
6	3.76×10^{1}	3.62×10^{0}	2.52×10^{1}	4.99×10^{0}	2.29×10^{1}	4.09×10^{0}	1.85×10^{1}	4.59×10^{0}	1.47×10^{1}	2.09×10^{0}	$\mathbf{1.26 \times 10^{1}}$	1.95×10^{0}
7	9.52×10^{-1}	8.96×10^{-2}	4.64×10^{-2}	3.78×10^{-2}	$\mathbf{4.03 \times 10^{-2}}$	2.61×10^{-2}	6.15×10^{-2}	3.31×10^{-2}	4.47×10^{-2}	2.32×10^{-2}	5.15×10^{-2}	3.13×10^{-2}
8	5.83×10^{2}	9.72×10^{1}	1.32×10^{2}	3.85×10^{1}	9.95×10^{1}	2.41×10^{1}	7.32×10^{1}	2.36×10^{1}	6.28×10^{1}	1.19×10^{1}	$\mathbf{2.48 \times 10^{1}}$	7.62×10^{0}
9	6.78×10^{2}	1.59×10^{2}	1.64×10^{2}	4.59×10^{1}	1.46×10^{2}	4.21×10^{1}	9.38×10^{1}	3.25×10^{1}	6.79×10^{1}	1.43×10^{1}	$\mathbf{4.36 \times 10^{1}}$	7.75×10^{0}
10	4.76×10^{2}	7.88×10^{1}	2.356×10^{2}	6.04×10^{1}	2.62×10^{2}	6.13×10^{1}	1.59×10^{2}	4.68×10^{1}	1.35×10^{2}	2.29×10^{1}	$\mathbf{8.83 \times 10^{1}}$	1.70×10^{1}
11	4.96×10^{3}	6.59×10^{2}	2.86×10^{3}	5.43×10^{2}	2.65×10^{3}	4.91×10^{2}	3.54×10^{3}	8.47×10^{2}	2.35×10^{3}	3.07×10^{2}	$\mathbf{2.12 \times 10^{3}}$	3.64×10^{2}
12	4.88×10^{3}	5.76×10^{2}	3.79×10^{3}	5.01×10^{2}	3.34×10^{3}	4.95×10^{2}	3.73×10^{3}	6.42×10^{2}	2.54×10^{3}	3.74×10^{2}	$\mathbf{2.45 \times 10^{3}}$	2.83×10^{2}
13	6.48×10^{-1}	2.91×10^{-1}	4.93×10^{-1}	2.51×10^{-1}	4.67×10^{-1}	3.28×10^{-1}	1.14×10^{-1}	7.21×10^{-2}	5.72×10^{-2}	2.11×10^{-2}	$\mathbf{4.78 \times 10^{-2}}$	1.83×10^{-2}
14	4.27×10^{2}	7.16×10^{1}	1.41×10^{2}	2.48×10^{1}	1.16×10^{2}	5.23×10^{1}	8.38×10^{1}	2.15×10^{1}	6.22×10^{1}	9.46×10^{0}	$\mathbf{3.07 \times 10^{1}}$	1.04×10^{1}
15	2.26×10^{2}	4.52×10^{1}	1.86×10^{2}	5.19×10^{1}	1.88×10^{2}	4.19×10^{1}	8.72×10^{1}	2.43×10^{1}	6.10×10^{1}	9.54×10^{0}	$\mathbf{5.04 \times 10^{1}}$	1.08×10^{1}
16	1.59×10^{1}	3.84×10^{0}	7.08×10^{0}	2.43×10^{0}	6.57×10^{0}	2.12×10^{0}	5.14×10^{0}	1.92×10^{0}	3.03×10^{0}	6.41×10^{-1}	$\mathbf{2.76 \times 10^{0}}$	4.93×10^{-1}
17	3.98×10^{2}	9.85×10^{1}	3.22×10^{2}	9.46×10^{1}	2.13×10^{2}	6.27×10^{1}	2.56×10^{2}	8.53×10^{1}	$\mathbf{2.00 \times 10^{2}}$	2.81×10^{-3}	$\mathbf{2.00 \times 10^{2}}$	1.42×10^{1}
18	6.41×10^{3}	1.32×10^{3}	3.53×10^{3}	7.58×10^{2}	3.31×10^{3}	6.30×10^{2}	4.31×10^{3}	8.92×10^{2}	3.15×10^{3}	3.79×10^{2}	$\mathbf{2.46 \times 10^{3}}$	4.17×10^{2}
19	6.39×10^{3}	7.98×10^{2}	4.69×10^{3}	8.97×10^{2}	4.45×10^{3}	7.88×10^{2}	4.31×10^{3}	7.67×10^{2}	3.10×10^{3}	5.17×10^{2}	$\mathbf{2.71 \times 10^{3}}$	3.97×10^{2}
20	3.96×10^{2}	7.53×10^{1}	2.80×10^{2}	1.38×10^{1}	2.65×10^{2}	2.17×10^{1}	2.54×10^{2}	1.74×10^{1}	2.36×10^{2}	1.20×10^{1}	$\mathbf{2.21 \times 10^{2}}$	1.10×10^{1}
21	4.28×10^{2}	3.19×10^{1}	2.96×10^{2}	1.21×10^{1}	2.92×10^{2}	1.25×10^{1}	2.85×10^{2}	1.33×10^{1}	2.69×10^{2}	1.96×10^{1}	$\mathbf{2.56 \times 10^{2}}$	5.47×10^{0}
22	4.32×10^{2}	9.84×10^{1}	2.72×10^{2}	8.51×10^{1}	2.15×10^{2}	4.17×10^{1}	2.11×10^{2}	2.81×10^{1}	$\mathbf{2.00 \times 10^{2}}$	1.75×10^{-2}	$\mathbf{2.00 \times 10^{2}}$	1.68×10^{-2}
23	1.59×10^{3}	1.31×10^{2}	9.89×10^{2}	1.39×10^{2}	8.70×10^{2}	2.09×10^{2}	8.17×10^{2}	1.23×10^{2}	6.85×10^{2}	9.76×10^{1}	$\mathbf{6.70 \times 10^{2}}$	7.61×10^{1}
24	4.79×10^{3}	2.38×10^{3}	4.42×10^{2}	4.69×10^{2}	2.91×10^{2}	5.39×10^{1}	3.58×10^{2}	2.59×10^{2}	$\mathbf{2.64 \times 10^{2}}$	7.57×10^{1}	2.94×10^{2}	0.11×10^{0}

4. Process Neural Network Model Optimized by ILoTFWA

The ILoTFWA was applied to the counter-propagation process neural network (CPPNN) to optimize the initial weights and thresholds. Using the measured data of experiment and operation data of the 300 MW generator, the effect was compared with the neural network models optimized by other algorithms to verify the feasibility of this method.

4.1. CPPNN Model

The CPPNN is a feed-forward network model with a three-layered structure, composed of an input layer, competition layer, and output layer. The adjacent layers of the neural nodes are fully interconnected, and the input layer has n nodes to complete the input of n time-varying functions to the network. There are h nodes in the competition layer, which is composed of process neurons and implements the generalized self-organizing mapping algorithm to complete the adaptive competition classification of input patterns. The output layer is composed of m general non-time-varying neuron nodes. The spatial aggregation operation of process neurons adopts the weighted sum, and the time accumulation operation adopts the integral; the network topology is shown in Figure 5. At the same time, further optimization of parameters such as weights should be considered to improve the performance of the CPPNN.

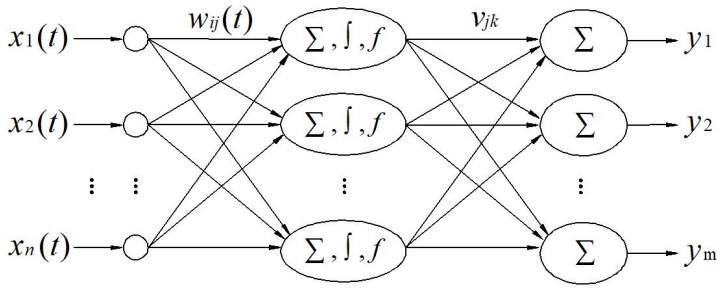


Figure 5. The CPPNN model.

$x_1(t)$, $x_2(t)$, … , $x_n(t)$ ($t \in [0, T]$) is the network input function; $w_{ij}(t)$ ($i = 1, 2, \ldots, n$; $j = 1,2, \ldots, H$) is the connection weight function from the input layer node i to the competitive layer node j; v_{jk} ($j = 1, 2, \ldots, H$; $k = 1, 2, \ldots, m$) is the connection weight between the competition layer and the output layer; y_k($k = 1, 2, \ldots, m$) is the network output; [0, T] is the input process interval; and f is the excitation function of process neurons.

During network training, training samples $X^1(t)$, $X^2(t)$, … , $X^n(t)$ are input in a certain or random order at the input end. The total weighted input signal from each node of the input layer to the process neuron node j of the competition layer is as follows:

$$s_j(t) = \sum_{i=1}^{n} w_{ij}(t) x_i(t) \ , \ j = 1, 2, \ldots, m \tag{7}$$

$b_1(t)$, $b_2(t)$, … , $b_k(t)$ … is a set of standard orthogonal basis functions in C [0, T], and $X(t) = (x_1(t), x_2(t), \ldots, x_n(t))$ are functions in the input space. Under the given fitting accuracy, $x_i(t)$ is expressed as a finite-term expansion of the basis function.

$$x_i(t) = \sum_{l=1}^{L} a_{il} b_l(t) \ , \ i = 1, 2, \ldots, n \tag{8}$$

In addition, the weight function $w_{ij}(t)$ is also expanded with $b_1(t)$, $b_2(t)$, … , b_L (t).

$$w_{ij}(t) = \sum_{l=1}^{L} w_{ij}^{(l)} b_l(t) \ , \ i = 1, 2, \ldots, n \ ; \ j = 1, 2, \ldots, m \tag{9}$$

where $w_{ij}^{(l)}$ is the connection weight between the input layer and the competition layer of $w_{ij}(t)$ relative to $b_l(t)$.

4.2. Structural Optimization Design of CPPNN Based on ILoTFWA

The weight and threshold of the network are the key factors that affect the prediction performance of the CPPNN model. The fireworks algorithm has the advantages of a simple mechanism and strong optimization ability. Therefore, the ILoTFWA based on the LoTFWA was introduced into the process neural network model to optimize the weight and threshold of the process neural network, so as to realize the most effective learning and prediction of the model. The whole flow chart of the ILoTFWA-CPPNN algorithm is shown in Figure 6.

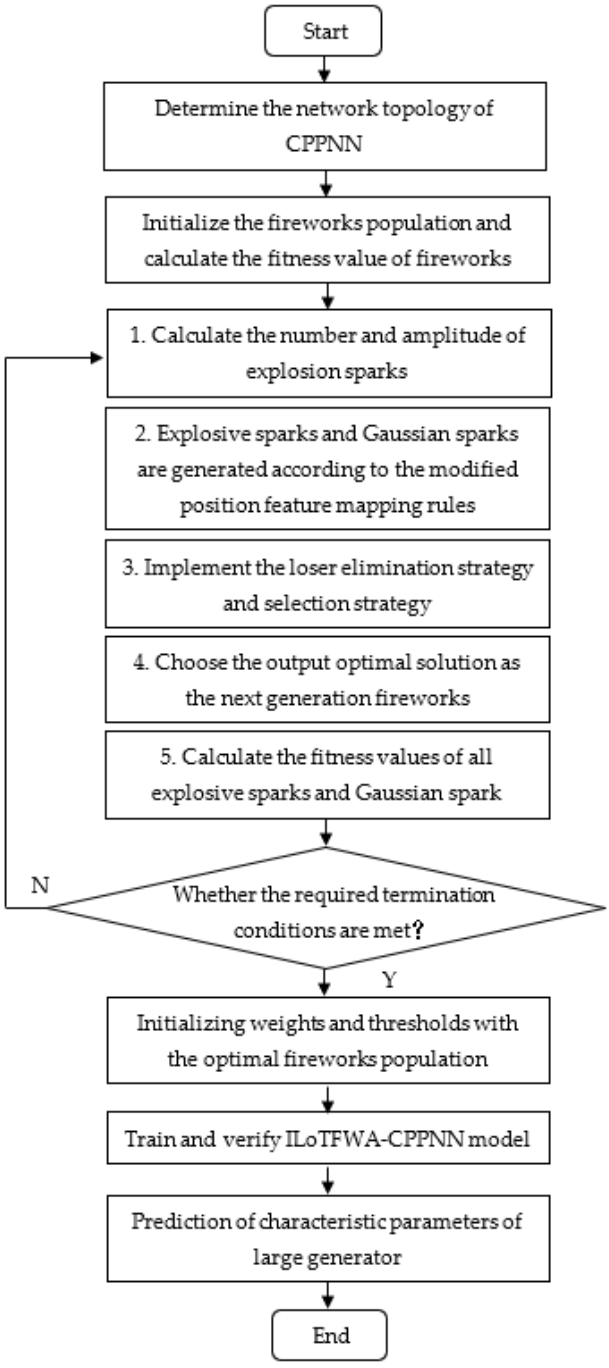


Figure 6. The flow chart of ILoTFWA-CPPNN algorithm.

4.3. Validation of ILoTFWA-CPPNN Algorithm Model

In this paper, 130 sets of steady-state asymmetric operation data for a No. 1 300 WM turbo-generator in a power plant, over a period of six months (March, April, May, June, July and August in 2019), were selected. Moreover, 104 samples constituted the training set and 26 samples constituted the test set. Comprehensively considering the design manual, daily operation data, maintenance records, and engineer's experience of a large generator, a three-phase current versus time curve, spatial geometric position versus time curve of main rotor components, thermal conductivity versus time curve, and conductivity versus time curve of rotor slot wedge were all selected as the input parameters. Through experimental comparison and analysis, the CPPNN network structure was selected as 6-15-1; that is, 6 input nodes, 15 process neuron nodes in the competitive layer, and 1 non-time-varying neuron output node. The output value is the maximum temperature rise of the main components of the rotor. The Walsh function was selected as the basis function. When the basis function item L = 16, the fitting accuracy of the input function was 0.01. Error accuracy was $\varepsilon = 0.05$ and maximum learning times M = 10,000. The ILoTFWA algorithm proposed in this paper was used to optimize the weight and threshold of the CPPNN, and the network converged after 2793 training cycles. Using the trained ILoTFWA-CPPNN model to calculate the samples in the training sample set, the average relative errors were 2.81%, respectively. The average relative error of 26 samples in the test set was 2.65%, which is a good result in the current prediction of rotor temperature rise.

In order to further verify the prediction performance of the model, the same data set was used to train the classical CPPNN, the genetic algorithm-improved CPPNN (GA-CPPNN), the particle swarm optimization algorithm-improved CPPNN (PSO-CPPNN), and the classical fireworks algorithm-improved CPPNN (FWA-CPPNN). At the same time, according to the specific optimization objectives of the weight and threshold and combined with the relevant experimental results, the key parameters of the three algorithms were set as follows. The population size of the classical fireworks algorithm was $n = 70$, the adjustment constant of fireworks explosion radius was $d = 5$, the adjustment constant of the firework explosion spark number was $c = 40$, the upper limit of the firework explosion spark number was $ub = 0.8$, the lower limit of the firework explosion spark number was $lb = 0.04$, the number of Gaussian variation sparks was $g = 5$, and the maximum number of iterations was $T = 1000$. The parameters of the GA were: population size $popu = 30$, genetic algebra $gen = 100$, crossover probability $pcross = 0.8$, and mutation probability $pmutation = 0.05$. For the PSO, the parameters were as follows: speed update parameter $c_1 = c_2 = 1.494\,45$, evolution number $maxgen = 150$, population size $sizepop = 30$, individual maximum $popmax = 7$, individual minimum $popmin = -7$, individual maximum speed $v_{max} = 1$, and individual minimum speed $v_{min} = -1$. For the parameter selection in the standard CPPNN network prediction model, the same parameters as the ILoTFWA-CPPNN model in this paper were used. For the steady-state experiment under asymmetric operating conditions, 300 MW generators of a power plant were used in the experiment as shown in Figure 7, and the details of the experiments are given in [45]. Some measured temperature-rise data of the rotors and the comparison results of various prediction models are shown in Table 3.

Table 3 indicates that the ILoTFWA-CPPNN method shows better performance in predicting the maximum temperature rise of the rotor, both in terms of the accuracy and learning time. The average error of the prediction results of the CPPNN model was 4.89%; the average error of the GA-CPPNN model was 3.68%; the average error of the PSO-CPPNN model was 3.49%; the average error of the FWA-CPPNN model was 3.63%; and the average error of the ILoTFWA-CPPNN was 2.57%. Therefore, among these neural network models, the ILoTFWA-CPPNN had the smallest error in solving prediction problems.

Meanwhile, it can be seen that the average iteration number of the CPPNN to reach the minimum target value of training was 4.7; the average iteration number of the GA-CPPNN and FWA-CPPNN was 3.9; and the average iteration number of the PSO-CPPNN was 3.8. Hence, compared with other neural network models, the iteration number of the

ILoTFWA-CPPNN decreased by 31.9%, 17.9%, and 15.8%, respectively. It can also be seen that although different algorithms all showed certain fluctuations in different test samples, the error rate of the ILoTFWA-CPPNN was lower than that of other existing algorithms on the whole. Therefore, the feasibility and accuracy of this algorithm are fully proven.



Figure 7. The 300 MW generator for negative-sequence experiment.

Table 3. The temperature-rise prediction results of ILoTFWA-CPPNN and other CPPNN models.

No.	Measured Value	Calculation Results of the Maximum Temperature Rise of Generator Rotor (°C)									
		CPPNN		GA-CPPNN		PSO-CPPNN		FWA-CPPNN		ILoTFWA-CPPNN	
		Value	Relative Error	Value	Relative Error	Value	Relative Error	Value	Relative Error	Value	Relative Error
1	30.4	31.9	4.9%	31.1	2.3%	31.6	3.9%	31.3	3.0%	30.9	1.6%
2	28.6	29.3	2.4%	29.5	3.1%	29.4	2.8%	29.4	2.8%	29.1	1.7%
3	32.2	33.6	4.3%	31.1	3.4%	32.9	2.2%	33.1	2.8%	32.9	2.2%
4	28.3	29.4	3.9%	29.5	4.2%	29.3	3.5%	29.5	4.2%	29.0	2.5%
5	29.7	31.2	5.1%	30.4	2.4%	30.6	3.0%	30.3	2.0%	30.4	2.4%
6	22.0	23.6	7.3%	22.9	4.1%	22.7	3.2%	23.2	5.5%	22.5	2.3%
7	38.1	40.9	7.3%	40.5	6.3%	40.8	7.1%	40.7	6.8%	40.2	5.5%
8	24.5	25.8	5.3%	25.1	2.5%	25.2	2.9%	25.3	3.3%	25.3	3.2%
9	35.4	37.1	4.8%	36.1	2.0%	36.8	4.0%	36.2	2.3%	36.2	2.3%
10	30.7	31.8	3.6%	28.7	6.5%	31.4	2.3%	31.8	3.6%	31.3	2.0%
Average relative error		4.89		3.68		3.49		3.63		2.57	
Average number of iterations		4.7		3.9		3.8		3.9		3.2	

5. Prediction and Analysis of Maximum Temperature Rise

The rotor temperature-rise prediction of a large generator under asymmetric operating conditions is an important indicator of online monitoring and plays a vital role in evaluating and predicting the operating state of the entire power internet of things. To analyze such problems, the symmetrical component method is generally used to decompose the three-phase asymmetric current into three components: positive sequence, negative sequence, and zero sequence. Typically, the neutral point of the generator is not grounded or grounded through impedance, and the influence of zero-sequence current is minimal. Therefore, the influence of negative-sequence current on generator heating and temperature rise is mainly considered.

The rotor slot wedge material has a great influence on the temperature-rise distribution. Even if the same type of generator uses different slot wedge materials, the resulting heat distribution is also different. In addition, the degree of asymmetry of the system, that is, the amplitude of negative-sequence current, also plays a decisive role in the distribution of the heating and burning points of the generator. Therefore, this paper adopts the prediction model of the ILoTFWA-CPPNN, takes a 300 MW generator in a power plant as the research object, calculates the maximum temperature rise caused by the negative-sequence current of different main structural components under different working conditions and different slot wedge materials, comprehensively monitors and predicts the overall operation state of the

generator, and provides a reference for the management and regulation of the ubiquitous power internet of things.

The rotor slot wedge is an important structural component that cannot be ignored in the design, manufacture, and actual operation of a generator. In order to prevent overheating and burn damage of the generator rotor during asymmetric operation, major motor plants have taken correspondingly different improvement measures for 300 MW generators. Practice has proven that the reasonable selection of the slot wedge plays a very obvious role in improving a large generator's ability to bear negative-sequence current. The eddy current path can be improved by installing copper conductors at the butt joint of slot wedges. An aluminum bronze slot wedge can improve the eddy current distribution at the rotor end and close to the big teeth when the generator operates asymmetrically. Similarly, other alloy slot wedges with high mechanical strength and good electrical conductivity can also achieve similar effects. However, the large generator rotor is forged from whole rotor steel (as shown in Figure 4), so the negative-sequence current flows not only on the slot wedge but also on the rotor teeth. Due to the asymmetry of the rotor structure, the presence of big teeth will make the current on the slot wedge and teeth present with uneven distribution. Therefore, it is necessary to study the temperature rise and its distribution law of the main structural parts when different slot wedge materials are used.

The 300 MW generator studied in this paper has 10% steady-state negative-sequence capacity. Therefore, this paper summarizes the distribution law of the maximum temperature rise of rotor components using different slot wedge materials through the systematic research and analysis of a turbo-generator under different negative-sequence component proportions, and applies negative-sequence currents with negative-sequence component proportions of 1% to 10%, respectively (i.e., I_2 = 1% I_N, I_2 = 2% I_N, . . . , I_2 = 10% I_N). In order to find out the change characteristics and effective law of slot wedge materials, this paper studied an aluminum slot wedge, a beryllium bronze slot wedge, and an aluminum bronze slot wedge. The prediction results of the maximum temperature rise based on the ILoTFWA-CPPNN model are shown in Table 4.

Table 4. The maximum temperature-rise prediction results, when negative-sequence component proportion changes from 1% to 10%, under the condition of using different wedge materials.

Position	Wedge Material	Negative-Sequence Component Proportion									
		1%	2%	3%	4%	5%	6%	7%	8%	9%	10%
Big tooth	Aluminum	12.4	12.6	12.9	13.3	13.7	14.5	15.8	17.4	19.5	23.1
	Beryllium bronze	15.2	15.4	15.7	16.0	16.6	17.7	19.1	20.8	23.0	27.1
	Aluminum bronze	19.0	19.1	19.4	19.8	20.5	21.8	23.3	24.9	26.8	30.4
Damping slot wedge	Aluminum	13.3	13.5	13.8	14.1	14.6	15.6	17.2	18.7	20.9	24.3
	Beryllium bronze	16.1	16.5	16.7	17.2	17.8	18.9	20.4	21.9	24.2	29.1
	Aluminum bronze	20.0	20.2	20.5	20.9	21.3	22.7	24.1	25.6	27.5	31.4
Slot wedge	Aluminum	3.5	3.6	3.8	4.2	4.6	5.6	6.9	8.6	10.7	14.5
	Beryllium bronze	6.7	6.8	7.1	7.4	7.9	9.2	10.6	12.1	14.3	18.0
	Aluminum bronze	10.3	10.4	10.6	10.9	11.5	13.1	14.7	16.3	18.4	22.6
Small tooth	Aluminum	2.9	3.1	3.4	3.8	4.3	4.8	6.1	7.5	9.6	13.7
	Beryllium bronze	5.8	6.0	6.3	6.7	7.4	8.1	9.4	10.8	12.7	16.8
	Aluminum bronze	9.1	9.3	9.6	9.8	10.9	12.2	13.6	15.2	17.1	21.5

The prediction results in Table 4 clearly indicate that even if the same slot wedge material and the same structure are used, the temperature rise caused by negative-sequence current does not change correspondingly. In a steady-state situation, the smaller the negative-sequence component, the smaller the temperature rise caused by it; the larger the negative-sequence component, the sharper the temperature rise caused by it. When the negative-sequence current varied between 1% and 5%, the difference in the temperature-rise estimate was approximately 1.3 °C. Similar situations also occurred in the range of 6%

to 10%, and the difference in temperature rise was approximately 9 °C. Through the data analysis of the above two cases, it can be seen that the growth of the same change range doubled several times.

Meanwhile, from the results in Table 4, the conclusion can be obtained that slot wedge materials have a great influence on the heating of the large generator's rotor. Under the same negative-sequence component, the temperature rise of the aluminum slot wedge was the smallest, followed by the beryllium bronze slot wedge. The temperature rise of the aluminum bronze slot wedge was the largest, approximately 3 °C higher than beryllium bronze and approximately 7 °C higher than aluminum. Therefore, in similar negative-sequence working conditions, the negative-sequence heating of a rotor caused by an aluminum bronze slot wedge is more serious. Therefore, in the selection process of slot wedge material, high thermal conductivity should be preferred. Aluminum bronze has the lowest thermal conductivity among the three, and the thermal conductivity of the aluminum slot wedge and beryllium bronze slot wedge are relatively close. Furthermore, conductivity should be considered in the selection process as the higher the conductivity of the slot wedge, the greater the eddy current loss density, which can easily cause the local high temperature of the slot wedge itself. Therefore, when thermal conductivity is the same or close, the slot wedge material with slightly lower conductivity should be selected. For example, the conductivity of the aluminum slot wedge is lower than that of beryllium bronze, which produces the lowest negative-sequence temperature rise and effectively improves the negative-sequence operation capacity. At the same time, when the negative-sequence component was 10% and the slot wedge material was aluminum bronze, the maximum temperature rise was 31.4 °C.

Finally, for the three commonly used slot wedge materials, considering the influence on negative-sequence loss and heating, thermal conductivity, conductivity, and other major factors, the best choice of slot wedge material for a 300 MW large generator is undoubtedly the LY12 aluminum slot wedge.

The hyperparameters set in this paper have been debugged many times according to the actual operation data characteristics of the generator, so that the model training effect is better and the convergence speed is faster, which effectively ensures that the ILoTFWA-CPPNN model will neither fail to fit nor overfit in the training stage; at the same time, the network can learn the data structure characteristics as quickly as possible. In the process of solving iteration, it shows better optimization ability and faster iteration speed. Therefore, on the whole, the ILoTFWA-CPPNN shows better optimization performance than other algorithms. To sum up, through the analysis and calculation of the ILoTFWA-CPPNN prediction model in this paper, the results can provide an effective basis for the application of online mathematical algorithms in large devices.

6. Conclusions

Firstly, in consideration of the development of power systems, this paper thoroughly analyzes the new problems and challenges faced by large power equipment and points out that intelligent computing is an effective method of solving such problems. The CPPNN prediction model was used to predict and evaluate the generator operation status and development trend from the perspective of negative-sequence temperature rise under asymmetric working conditions. Aiming at the limitations of the CPPNN model, the FWA was improved. The weights and thresholds of the neural network were optimized by the ILoTFWA, and the ILoTFWA-CPPNN algorithm model was proposed. After 24 standard test function simulation experiments and in-depth analysis and verification of 300 MW generator measured data, the effectiveness and accuracy of this method were fully confirmed.

Secondly, the ILoTFWA-CPPNN model was adopted to analyze and calculate typical working conditions, such as different negative-sequence component proportions and different slot wedge materials. The maximum temperature rise caused by the negative-sequence current of each part of the rotor was calculated in detail when the negative-sequence

component changed from 1% to 10% and when the slot wedge material was aluminum, beryllium bronze, and aluminum bronze, respectively. The analysis of the calculation results shows that the rotor temperature-rise results are different when different slot wedge materials are used. The highest temperature rise occurred when aluminum bronze slot wedges were used, and the highest temperature rise under various negative-sequence proportions also occurred at this time. Additionally, the highest temperature-rise point appeared at the slot wedge on the polar surface of the rotor when the aluminum bronze slot wedge was used, and the temperature of the trunking near the big tooth was higher. When other slot wedge materials were replaced, the temperature rise of all parts of the rotor was greatly reduced. The lowest negative-sequence temperature rise in the whole rotor domain occurred when the rotor slot wedge was made of aluminum slot wedge material. Therefore, it is concluded that the slot wedge material has a great influence on rotor heating under different negative-sequence component proportions.

Thirdly, according to the analysis and calculation results of the influence of different slot wedge materials on the loss and temperature rise of the generator rotor, the thermal conductivity, conductivity, eddy current density and other factors of the three most commonly used slot wedge materials were comprehensively considered and compared, and it is concluded that the best choice for a 300 MW steam turbine generator slot wedge material is to use a duralumin slot wedge, and a damping copper bar or copper alloy material can be considered for the rotor end and the slot wedge. This conclusion can provide a theoretical research basis for a turbo-generator with the same structure or similar rotor structure. At the same time, the ILoTFWA-CPPNN model proposed in this paper provides a feasible reference for the analysis of asymmetric working conditions of large power equipment.

Author Contributions: Conceptualization, W.G. and J.G.; methodology, W.G.; software, J.G.; validation, W.G. and F.M.; formal analysis, W.G.; investigation, F.M.; resources, J.G.; data curation, W.G.; writing—original draft preparation, W.G. and J.G.; writing—review and editing, W.G. and F.M.; visualization, J.G.; supervision, W.G.; project administration, J.G.; funding acquisition, J.G. All authors have read and agreed to the published version of the manuscript.

Funding: This research was funded by the Special Research Project of Basic Business in Colleges and Universities (Grant No. 145209147 and 135509212) and the Provincial Platform Opening Project (Grant No. WNCGQJKF202101) of Heilongjiang Province of China.

Institutional Review Board Statement: Not applicable.

Informed Consent Statement: Not applicable.

Data Availability Statement: The data presented in this study are available on request from the corresponding author.

Acknowledgments: The authors appreciate the financial support from the Heilongjiang Provincial Government of China and acknowledge the technical support from the Electric Machinery Company and Electric Power Design Institute for this work.

Conflicts of Interest: The authors declare no conflict of interest. The funders had no role in the design of the study; in the collection, analyses, or interpretation of data; in the writing of the manuscript; or in the decision to publish the results.

References

1. Zhou, Z.T.; Li, H.; Yang, Y.; Zhang, H.B.; Fan, Z.N. Real-Time Monitoring System for Rotor Temperature of a Large Turbogenerator Based on SmartMesh IP Wireless Network Communication Technology. *China Commun.* **2022**, *19*, 150–163. [CrossRef]
2. Tappura, K.; Juntunen, T.; Jaakkola, K.; Ruoho, M.; Tittonen, I.; Ritasalo, R.; Pudas, M. Large-area implementation and critical evaluation of the material and fabrication aspects of a thin-film thermoelectric generator based on aluminum-doped zinc oxide. *Renew. Energy* **2020**, *147*, 1292–1298. [CrossRef]
3. Zhu, Y.X.; Newbrook, D.W.; Dai, P.; Kees, C.H.; Huang, R.M. Artificial neural network enabled accurate geometrical design and optimisation of thermoelectric generator. *Appl. Energy* **2022**, *305*, 117800. [CrossRef]
4. Xie, X.D.; Wen, S.P.; Zeng, Z.G.; Huang, T.W. Memristor-based circuit implementation of pulse-coupled neural network with dynamical threshold generators. *Neurocomputing* **2018**, *284*, 10–16. [CrossRef]

5. Jin, X.; Chen, Y.M.; Wang, L.; Han, H.L.; Chen, P. Failure prediction, monitoring and diagnosis methods for slewing bearings of large-scale wind turbine: A review. *Measurement* **2021**, *172*, 108855. [CrossRef]
6. Tekerek, A.; Kurt, E. Artificial neural network analysis on an axial flux permanent magnet generator having variable air gap and power regime. *Sadhana Acad. Proc. Eng. Sci.* **2021**, *46*, 240. [CrossRef]
7. Sumathi, S.; Bansilal. Artificial Neural Network for coordinated control of STATCOM, generator excitation and tap changing transformer. *J. Renew. Sustain. Energy* **2015**, *64*, 536–541. [CrossRef]
8. Shariati, O.; Aghamohammadi, M.R.; Potter, B. On-Line Determination of Salient-Pole Hydro Generator Parameters by Neural Network Estimator Using Operating Data (PEANN). *IEEE Access* **2021**, *9*, 134638–134648. [CrossRef]
9. Siddiqui, S.A.; Verma, K.; Niazi, K.R.; Fozdar, M. Real-Time Monitoring of Post-Fault Scenario for Determining Generator Coherency and Transient Stability through ANN. *IEEE Trans. Ind. Appl.* **2018**, *54*, 685–692. [CrossRef]
10. Sharifi, A.; Sharafian, A.; Ai, Q. Adaptive MLP neural network controller for consensus tracking of Multi-Agent systems with application to synchronous generators. *Expert Syst. Appl.* **2021**, *184*, 115460. [CrossRef]
11. Wang, T.C.; Wang, J.Y.; Wu, Y.; Sheng, X. A fault diagnosis model based on weighted extension neural network for turbo-generator sets on small samples with noise. *Chin. J. Aeronaut.* **2020**, *33*, 2757–2769. [CrossRef]
12. Duan, Y.Z.; He, X. A Non-convex Dispatch Problem with Generator Constraints Using Neural Network and Particle Swarm Optimization. *Iran. J. Sci. Technol. Trans. Electr. Eng.* **2020**, *44*, 185–196. [CrossRef]
13. Yan, D.F.; Hu, B. Shared Representation Generator for Relation Extraction with Piecewise-LSTM Convolutional Neural Networks. *IEEE Access* **2019**, *12*, 31672–31680. [CrossRef]
14. Yao, F.J.; Zhao, J.B.; Li, X.J.; Mao, L.; Qu, K.Q. RBF Neural Network Based Virtual Synchronous Generator Control with Improved Frequency Stability. *IEEE Trans. Ind. Inform.* **2021**, *17*, 4014–4024. [CrossRef]
15. Wang, F.; Bao, W.; Wang, Y.; Wang, X.; Ren, K.; Wang, Z.; Li, J. Ejection state prediction for a pneumatic micro-droplet generator by BP neural networks. *J. Adv. Mech. Des. Syst. Manuf.* **2020**, *14*, JAMDSM0001. [CrossRef]
16. Quan, Q.; Zhang, Z.Q. Supply Capability Evaluation of Intelligent Manufacturing Enterprises Based on Improved BP Neural Network. *J. Math.* **2022**, *2022*, 8572424. [CrossRef]
17. Jin, X.H.; Xu, Z.W.; Qiao, W. Condition Monitoring of Wind Turbine Generators Using SCADA Data Analysis. *IEEE Trans. Sustain. Energy* **2021**, *12*, 202–210. [CrossRef]
18. Kreischer, C. Modern methods to monitor end winding vibrations in turbo-generators. *Compel Int. J. Comput. Math. Electr. Electron. Eng.* **2019**, *38*, 1214–1223. [CrossRef]
19. Sawant, S.S.; Wiedmann, M.; Gob, S.; Holzer, N.; Lang, E.W.; Gotz, T. Compression of Deep Convolutional Neural Network Using Additional Importance-Weight-Based Filter Pruning Approach. *Appl. Sci.* **2022**, *12*, 11184. [CrossRef]
20. Ghazvini, M.; Varedi-Koulaei, S.M.; Ahmadi, M.H.; Kim, M. Optimization of MLP neural network for modeling flow boiling performance of Al_2O_3/water nanofluids in a horizontal tube. *Eng. Anal. Bound. Elem.* **2022**, *7*, 3214–3221. [CrossRef]
21. Haddadi, A.; Zhao, M.X.; Kocar, I.; Karaagac, U.; Chan, K.W.; Farantatos, E. Impact of Inverter-Based Resources on Negative Sequence Quantities-Based Protection Elements. *IEEE Trans. Power Deliv.* **2021**, *36*, 289–298. [CrossRef]
22. Li, L.; Chen, M.; Wang, F.; Xu, A.A. The Influence of Rotor Adjustment Parameters on the Dynamic Balance of a Scale-Model Rigid Variable Speed Rotor. *Appl. Energy* **2022**, *12*, 12125. [CrossRef]
23. Zhang, Y.C.; Kang, C.; Zhao, H.X.; Teng, S. Effects of in-line configuration of drag-type hydrokinetic rotors on inter-rotor flow pattern and rotor performance. *Energy Convers. Manag.* **2019**, *196*, 44–55. [CrossRef]
24. Gulbahce, M.O.; Mcguiness, D.T.; Kocabas, D.A. Shielded axially slitted solid rotor design for high-speed solid rotor induction motors. *IET Electr. Power Appl.* **2018**, *12*, 1371–1377. [CrossRef]
25. Schreier, L.; Bendl, J.; Chomat, M. Analysis of stator and rotor currents and torque of induction machine with rotor-bar faults. *Electr. Eng.* **2020**, *103*, 519–528. [CrossRef]
26. Ghazvini, M.; Maddah, H.; Peymanfar, R.; Ahmadi, M.H.; Kumar, R. Experimental evaluation and artificial neural network modeling of thermal conductivity of water based nanofluid containing magnetic copper nanoparticles. *Phys. A Stat. Mech. Its Appl.* **2020**, *551*, 124127. [CrossRef]
27. Liu, Z.P.; Zhang, L. A review of failure modes, condition monitoring and fault diagnosis methods for large-scale wind turbine bearings. *Measurement* **2020**, *149*, 107002. [CrossRef]
28. He, X.G.; Xv, S.H. *Process Neural Network*, 1st ed.; Science Press: Beijing, China, 2007; pp. 18–24, 40–51, 147–150.
29. Lin, C.H. Wind Turbine Driving a PM Synchronous Generator Using Novel Recurrent Chebyshev Neural Network Control with the Ideal Learning Rate. *Energies* **2016**, *9*, 441. [CrossRef]
30. Xu, W.; Mohammed, O.M.E.; Liu, Y.; Islam, M.R. Negative Sequence Voltage Compensating for Unbalanced Standalone Brushless Doubly-Fed Induction Generator. *IEEE Trans. Power Electron.* **2020**, *359*, 667–680. [CrossRef]
31. Huang, Y.C.; Chen, L.; Huang, X.W.; Du, X.Z.; Yang, L.J. Performance of natural draft hybrid cooling system of large scale steam turbine generator unit. *Appl. Therm. Eng.* **2017**, *122*, 227–244. [CrossRef]
32. Tan, Y.; Ding, J. *Recent Advances in Fireworks Algorithm*, 1st ed.; Science Press: Beijing, China, 2015; pp. 1–21.
33. Ouyang, H.B.; Wei, W.Q.; Li, S.V.; Zhao, X.B.; Zou, D.X. A modified fireworks algorithm with dynamic search interval based on closed-loop control. *Math. Comput. Simul.* **2022**, *200*, 329–360.
34. Han, S.F.; Zhu, K.; Zhou, M.C.; Liu, X.J.; Liu, H.Y.; Al-Turki, Y.; Abusorrah, A. A Novel Multiobjective Fireworks Algorithm and Its Applications to Imbalanced Distance Minimization Problems. *IEEE CAA J. Autom. Sin.* **2022**, *9*, 1476–1489. [CrossRef]

35. Yu, J.Y.; Guo, J.S.; Zhang, X.F.; Zhou, C.H.; Xie, T.; Han, X. A Novel Tent-Levy Fireworks Algorithm for the UAV Task Allocation Problem under Uncertain Environment. *IEEE Access* **2022**, *10*, 102373–102385. [CrossRef]
36. Li, J.; Tan, Y. Loser-Out Tournament-Based Fireworks Algorithm for Multimodal Function Optimization. *IEEE Trans. Evol. Comput.* **2018**, *22*, 679–691. [CrossRef]
37. Guo, W.; Ge, B.; Gao, Y.; Li, M. Negative-sequence component analysis of an AP1000 nuclear turbo-generator in an internal short-circuit condition. *Electr. Power Compon. Syst.* **2015**, *43*, 633–643. [CrossRef]
38. Cao, J.; Wang, D.; Wang, Q.M.; Yuan, X.L.; Wang, K.; Chen, C.L. Network Attack Detection Method of the Cyber-Physical Power System Based on Ensemble Learning. *Appl. Sci.* **2022**, *12*, 6498. [CrossRef]
39. Camacho, A.; Castilla, M.; Miret, J.; Velasco, M.; Guzman, R. Positive-Sequence Voltage Control, Full Negative-Sequence Cancellation, and Current Limitation for Static Compensators. *IEEE J. Emerg. Sel. Top. Power Electron.* **2021**, *9*, 6613–6623. [CrossRef]
40. Kou, G.F.; Jordan, J.; Cockerham, B.; Patterson, R.; VanSant, P. Negative-Sequence Current Injection of Transmission Solar Farms. *IEEE Trans. Power Deliv.* **2020**, *35*, 2740–2743. [CrossRef]
41. Ni, J.K.; Shi, P. Global Predefined Time and Accuracy Adaptive Neural Network Control for Uncertain Strict-Feedback Systems with Output Constraint and Dead Zone. *IEEE Trans. Syst. Man Cybern. Syst.* **2021**, *51*, 7903–7918. [CrossRef]
42. Li, J.; Zheng, S.; Tan, Y. Adaptive Fireworks Algorithm. *Evol. Comput.* **2014**, *7*, 3214–3221.
43. Zheng, S.; Li, J.; Janecek, A. A cooperative framework for fireworks algorithm. *IEEE ACM Trans. Comput. Biol. Bioinform.* **2017**, *14*, 27–41. [CrossRef] [PubMed]
44. Li, J.; Zheng, S.; Tan, Y. The Effect of Information Utilization: Introducing a Novel Guiding Spark in the Fireworks Algorithm. *IEEE Trans. Evol. Comput.* **2017**, *21*, 153–166. [CrossRef]
45. Guo, W.; Guo, J. Rotor transverse slots' influence on negative sequence loss and heat distribution prediction of large generators based on Improved Radial Basis Function Process Neural Network. *Math. Probl. Eng.* **2022**, *2022*, 1865380. [CrossRef]

Disclaimer/Publisher's Note: The statements, opinions and data contained in all publications are solely those of the individual author(s) and contributor(s) and not of MDPI and/or the editor(s). MDPI and/or the editor(s) disclaim responsibility for any injury to people or property resulting from any ideas, methods, instructions or products referred to in the content.